Excited-State Intramolecular Proton Transfer: A Survey of TDDFT and RI-CC2 Excited-State Potential Energy Surfaces

Adelia J. A. Aquino* and Hans Lischka*

Institute for Theoretical Chemistry, Währingerstrasse 17, University of Vienna, A-1090 Vienna, Austria

Christof Hättig

Institute of Nanotechnology, Forschungszentrum Karlsruhe, P.O. Box 3640, D-76021 Karlsruhe, Germany

Received: January 17, 2005; In Final Form: February 10, 2005

TDDFT and RI-CC2 calculations have been performed on the excited-state intramolecular proton transfer in malonaldehyde, *o*-hydroxybenzaldehyde, salicylic acid, 7-hydroxy-1-indanone, and 2-(2′-hydroxyphenyl)-benzothiazole. Vertical and adiabatic excitation energies have been computed for the nπ^* and $\pi\pi^*$ states. Overall, we have found that both RI-CC2 and TDDFT methods are good candidates for the description of ESIPT potential energy surfaces. Proton transfer (PT) curves have been computed for both excited states. An essentially barrierless and very shallow energy profile has been found for the $\pi\pi^*$ state. For the nπ^* state the keto minimum is more pronounced than for the $\pi\pi^*$ state and, depending on the case, energy barriers ranging from values <0.1 eV up to 0.5 eV were found. From the computed PT curves we conclude that extended crossing regions between the two excited states will occur.

I. Introduction

Excited-state intramolecular proton transfer (ESIPT) is of great interest in photochemistry and photobiology. Many applications in such diverse areas as, e.g., laser dye,[1−3] UV filters,[4,5] or photostabilizers[6] are controlled by these processes. The proton-transfer dynamics has been studied extensively in the past by means of femtosecond laser experiments. For an overview of experimental work see, e.g., ref 7. The explanation and understanding of the ESIPT requires detailed knowledge of excited-state energy surfaces as a first prerequisite for the treatment of its photodynamics. The calculation of energy surfaces in electronically excited states is still a formidable task considering especially the large size of the molecules, which are of practical interest here. Because of the possibility of surface crossings and conical intersections, the appropriate methodological approach would be to use multireference methods. Such investigations have been performed at the complete active space self-consistent field (CASSCF) and complete active space perturbation theory to second order (CASPT2)[8] as well as at the multireference configuration interaction with singles and doubles (MR-CISD)[9] and multireference averaged quadratic coupled cluster (MR-AQCC)[9] levels. However, required computer times for such calculations are very large and limit these kinds of investigations to benchmark examples. Conceptually simpler and more economic methods such as density functional theory (DFT) are required for the investigation of the excited states of larger molecules. The time-dependent (TD) DFT version has been applied successfully for excited-state calculations in the investigations carried out by Sobolewski and Domcke[8] on a series of molecular systems (*o*-hydroxybenzaldehyde (OHBA), salicylic acid (SA), and 7-hydroxy-1-indanone (7HIN)) showing ESIPT. For a current review see ref 10. A very interesting investigation has been performed by Vivie-Riedle et al.[11] on a much larger compound, the 2-(2′-hydroxyphenyl)benzothiazole (HBT), using configuration interaction with single excitations (CIS) and TDDFT.

Major methodological progress has been achieved by the variational formulation of the TDDFT method by Furche and Ahlrichs[12] facilitating the calculation of analytic TDDFT gradients, thus allowing geometry optimizations in excited states. Despite the overwhelming success of DFT one should not forget its shortcomings, which led to the development of a large number of functionals. Concerning problems, we want to mention only the case of electron transfer[13] for which current DFT methods fail. So far, much more experience concerning the applicability of DFT is available for the electronic ground state than for the excited states. The possibilities and limits of TDDFT are much less documented. Therefore, support for TDDFT by ab initio methods is highly desirable. The CASSCF, CASPT2, and MR-AQCC methods have already been mentioned above. The approximate coupled cluster singles and doubles method (CC2)[14] is a very interesting alternative. The recent introduction of linear response theory (LRT) in combination with analytic gradients[15] provides the required possibilities for the treatment of excited states. The implementation of the resolution of the identity (RI) method[16] allows the efficient treatment of larger molecules. However, it should be noted that neither the TDDFT nor the CC2 methods are applicable in the case of avoided crossings or conical intersections where the single-reference approach breaks down.

The purpose of this paper is to perform a survey on the applicability of the TDDFT method to ESIPT processes by using several functionals and to compare the obtained results with those of the RI-CC2 method. Furthermore, comparison is made to available CASPT2 and MR-AQCC results. We have chosen the aforementioned molecules MA, OHBA, SA, and 7HIN as a set of medium-sized benchmark molecules. Finally, HBT has been chosen as an example for a significantly larger system. It is a major goal to demonstrate that for such systems excited-

* Address corrsespondence to these authors. E-mail: adelia.aquino@univie.ac.at, hans.lischka@univie.ac.at.

10.1021/jp050288k CCC: $30.25
Published on Web 03/17/2005

state surfaces can be computed both efficiently and reliably. Besides vertical and adiabatic excitation and fluorescence processes, the proton transfer (PT) is the major focus of our work. Whereas the PT in the $\pi\pi^*$ state has been investigated quite intensively (see, e.g., refs 8 and 11), much less is known about these processes in the $n\pi^*$ state. The question whether surface crossings occur in the course of the PT is a very important one for the photodynamics, but also a very practical one in view of the breakdown of the TDDFT and CC2 methods at conical intersections. The future goal of our investigations is the performance of dynamics calculations for which reliable energy surfaces are required. The present calculations should set the first step leading to benchmark results to be used for fitting parameters of semiempirical methods, which, following the work of Granucci et al.,[17] can be used for on-the-fly quasiclassical surface-hopping dynamics calculations of ESIPT processes. This combined ab initio/semiempirical approach has already been used successfully in modeling the excited-state surfaces of ethylene[18] allowing extensive surface-hopping simulations of this system.

II. Computational Details

The TURBOMOLE program package[19] has been used for the TDDFT[12,20,21] and RI-CC2[15,16] calculations. The two functionals B3LYP[22] and PBE[23] have been tested. The performance of the latter nonhybrid method is of special interest since the RI method can be applied in this case for reducing the computational effort considerably. The SVP,[24] TZVP,[25] and TZVPP[25] basis sets have been used. The SVP basis is the smallest basis used here. This basis is sufficiently small to allow cost-effective calculations on larger compounds. The TZVP and TZVPP basis sets are of triple-ζ quality. The last one contains two d sets and one f set on the heavy atoms and two p functions and one d function on the hydrogen atom. The RI basis set used in the RI-CC2 calculations is described in ref 26.

Following the work of Sobolewski and Domcke,[27] the coordinate-driven minimum-energy path approach has been chosen for the construction of the ESIPT reaction path. The reaction coordinate is defined as $R_- = {}^1/_2(R_{OH} - R_{XH})$, where O is the hydroxyl oxygen and X is the proton acceptor atom oxygen or nitrogen. For a given value of R_{OH} all other internal coordinates have been optimized. In the case of MA only the symmetry-unique part of the reaction path has been calculated explicitly. All molecules investigated are depicted in Figure 1. C_s symmetry of the nuclear framework has been imposed in all cases. The stationary points have been characterized by a harmonic analysis.

Radiative lifetimes have been computed for spontaneous emission by using the Einstein transition probabilities according to the formula (in au)[28]

$$\tau = \frac{c^3}{2(\Delta E)^2 f} \qquad (1)$$

where c is the velocity of light, ΔE is the transition energy, and f is the oscillator strength.

III. Proton Transfer Curves and Excitation Energies

Searches for stationary points and geometry optimizations have been performed for the electronic ground state and for the $n\pi^*$ and $\pi\pi^*$ states. In the ground state energy minima have been found only for the enol form. Searches for ground-state minima on the keto side have been carried out also starting from the keto structure of the excited state. However, geometry optimizations always led back to the enol form. In agreement with this finding, ground-state PT transfer curves computed in the same way as for the ESIPT showed barrierless reaction paths to the enol form. Thus, we conclude that for the systems investigated here no local keto minima exist for the ground state. In the case of the excited states, the locations of stationary points and PT curves are discussed below.

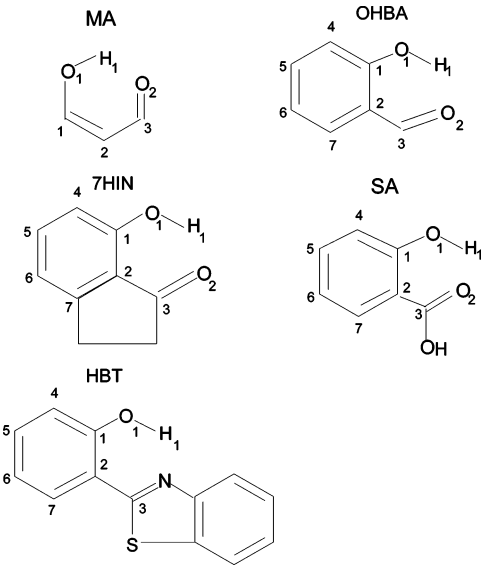

Figure 1. Investigated molecules and atomic numbering scheme.

A. Malonaldehyde. MA has C_s symmetry in the ground state.[29] Geometry optimization of the $\pi\pi^*(2^1A')$ state at the CASPT2 level restricted to planar structures gave a symmetrical C_{2v} structure as the most stable one.[27] At the CASSCF level relatively large active spaces had to be used to reproduce this result. The energy minimum of the $n\pi^*(1^1A'')$ state possesses C_s symmetry. The C_{2v} structure is a saddle point for the hydrogen transfer. Distortion of the C_{2v} structures along an a_2 vibrational mode leads to a coupling of both states and results in the true saddle point for the PT.

PT curves computed with the TDDFT and RI-CC2 methods are displayed in Figure 2. For the $1^1A''(n\pi^*)$ state the situation is clear. There is a well-defined C_s minimum structure with an energy barrier of about 0.2 (RI-CC2) and 0.3 eV (B3LYP), respectively. The RI-CC2 and B3LYP curves are relatively close to each other, whereas the PBE curve is located energetically lower by about 0.4 eV. The CASPT2 barrier between the C_s and C_{2v} structures is 0.51 eV,[27] and the MR-AQCC calculations[9] give a value of 0.40 eV. Thus, all methods used here underestimate the energy barrier by about 0.2−0.3 eV. For the $2^1A'(\pi\pi^*)$ state, the curves shown in Figure 2 have a very shallow double minimum in the proton-transfer coordinate for B3LYP and PBE, in disagreement with the just-mentioned CASPT2 and MR-AQCC calculations, where a single minimum of C_{2v} symmetry was found. RI-CC2 gives a single minimum in agreement with the other ab initio results.

The energetic results for MA are presented in Table 1. In almost all cases, basis set effects are around 0.1 eV or smaller. For the $n\pi^*$ state PBE gives the best agreement with experimental vertical excitation energies. The target value for the m-m excitation energy of the $n\pi^*$ state is about 3.50−3.60 eV. This energy range is obtained from the experimental 0−0 transition and with zero-point energy corrections of 0.15 eV (CASSCF frequencies of ref 27) and 0.06 (this work). Thus, the CASPT2 method seems to have a slight tendency to underestimate excitation energies. The PBE method gives m-m excitation

TABLE 1: TDDFT and RI-CC2 Vertical (vert) and Minimum-to-Minimum (m-m) and Zero-Point Corrected (0−0) Absorption Energies (eV) for MA Relative to the Ground-State Energy Minimum, Oscillator Strengths, and Radiative Lifetimes[a]

geometry	transition[b]	B3LYP SVP/TZVPP	PBE SVP/TZVPP	RI-CC2 SVP/TZVPP	CASPT2[c]/ MR-AQCC[d] (exptl)
gr.st.(C_s)	vert(nπ*)	4.01/3.93	3.69/3.60	4.17/4.00	3.82/3.76 (3.6[e])
gr.st.(C_s)	vert($\pi\pi$*)	5.18/5.11/ (0.20/0.21)	5.00/4.91 (0.18/0.18)	5.05/4.89	4.51/4.86 (4.7[e])
nπ*(C_s)	m-m(nπ*)	3.69/3.63	3.29/3.21	3.69/3.50	3.38/3.70
	0−0(nπ*)	3.63			(3.44[f])
$\pi\pi$*(C_s)	m-m($\pi\pi$*)	4.95/4.88	4.80/4.71	4.54/4.43	3.95/4.40
	0−0(nπ*)	4.81			
nπ*(C_s)	fl(nπ*)[g]	3.29/3.24	2.70/2.67	2.99/2.74	2.72
$\pi\pi$*(C_s)	fl($\pi\pi$*)[g]	4.71/4.65 (5.77/5.92)	4.60/4.52 (6.80/7.05)	4.22/4.14	
nπ*(C_s)	st(nπ*)[h]	0.72/0.69	0.99/0.93	1.18/1.26	1.10
$\pi\pi$*(C_s)	st($\pi\pi$*)[h]	0.47/0.46	0.40/0.39	0.83/0.75	

[a] Oscillator strengths (absorption) and radiative lifetimes (ns) for fluorescence are given in parentheses for vertical $\pi\pi$* transitions. Oscillator strengths for nπ* transitions are less than 10^{-3} and are not given in the table. [b] n-π*(C_s): 1^1A", $\pi\pi$*(C_s): 2^1A′, nπ*(C_{2v}): 1^1B_1, $\pi\pi$*(C_{2v}): 1^1B_2. [c] Reference 11. [d] Reference 12. [e] Reference 35. [f] Reference 36. [g] fl denotes vertical fluorescence transitions from the excited state to S_0. [h] st denotes the Stokes shift.

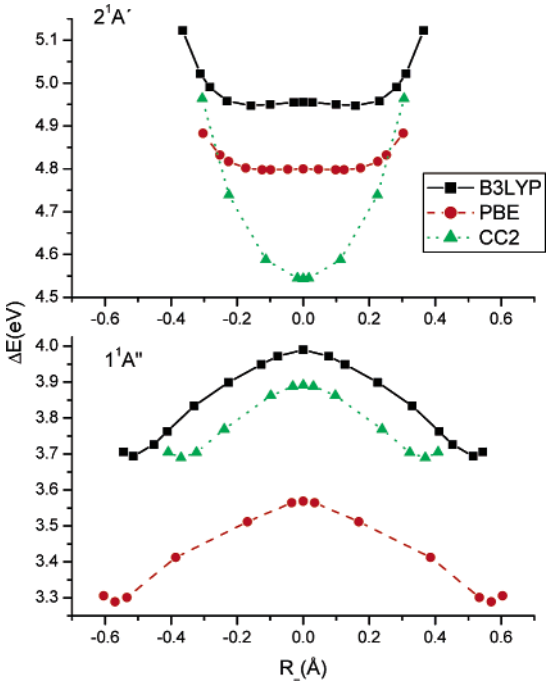

Figure 2. Proton-transfer curves for MA. Energies are given relative to the ground-state energy minimum.

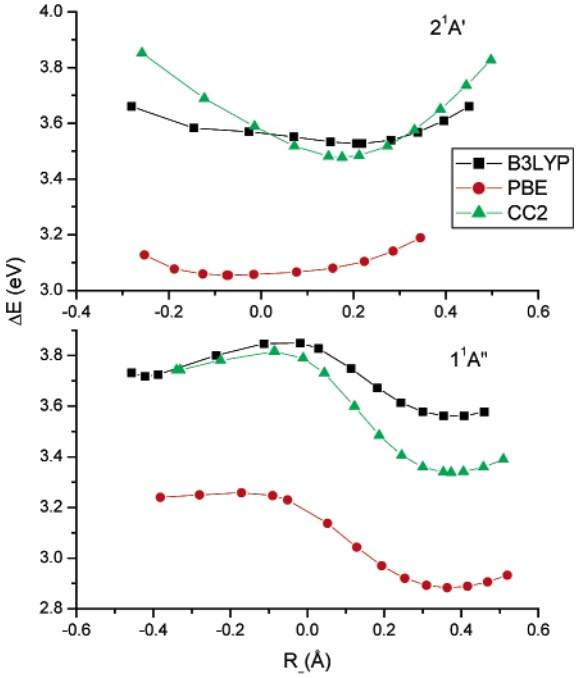

Figure 3. Proton-transfer curves for OHBA. Energies are given relative to the ground-state energy minimum.

energies which are too small by about 0.3 eV. Both the B3LYP and RI-CC2 methods are quite close to the target value. The MR-AQCC energy of the C_{2v} structure is 4.10 eV above the ground state (as compared to the CASPT2 value of 3.89 eV). Thus, the whole PBE curve is energetically too low whereas the B3LYP and RI-CC2 curves give a better energetic representation.

For the $\pi\pi$* state all methods used here give vertical excitation energies, which are too high by at least 0.2 eV. B3LYP values are the highest ones. B3LYP and PBE also give m-m excitation energies, which are too high by about 0.3−0.5 eV in comparison to the MR-AQCC value, whereas RI-CC2 gives good agreement with the MR-AQCC results. From a comparison of CASPT2 and MR-AQCC results for the m-m excitation energy (3.95 eV vs 4.40 eV) we conclude that the former results are probably too low. Thus, the relatively large discrepancy of 1 eV between the TDDFT and CASPT2 results noted in ref 8 is partly due to a too low CASPT2 excitation energy. Concerning fluorescence data, B3LYP values for the nπ* state are too high in comparison with the CASPT2 result. For the $\pi\pi$* state no reference values are available.

B. *o*-Hydroxybenzaldehyde. The proton-transfer curves for OHBA are displayed in Figure 3. Excitation energies are given in Table 2. For the nπ* state two minima are found: a very shallow one for the enol form and a pronounced one for the keto form. For the $\pi\pi$* state the B3LYP and PBE curves are very flat as well, the PBE minimum being on the enol side. The RI-CC2 curve is steeper. The minimum is located slightly on the keto side. Similar shallow curves have been obtained by CASSCF and CASPT2 calculations.[8]

The B3LYP and RI-CC2 $\pi\pi$* excitation energies agree well with CASPT2 and experimental data, with B3LYP even doing better. The PBE values are mostly too low. In the case of the

TABLE 2: TDDFT and RI-CC2 Vertical (vert) and Minimum-to-Minimum (m-m) and Zero-point Corrected (0−0) Absorption Energies (eV) for OHBA Relative to the Ground-State Energy Minimum, Oscillator Strengths, and Radiative Lifetimes[a]

geometry	transition[b]	B3LYP SVP/TZVP	PBE SVP	RI-CC2 SVP/TZVP	CASPT2[c] (exptl)
gr.st.	vert($\pi\pi^*$)	3.92/3.94 (0.07/0.07)	3.44 (0.05)	4.15/4.10	3.74 (3.9,[d,e] 3.8[f])
gr.st.	vert(nπ^*)	3.97/3.96	3.52	4.18/4.08	3.91
$\pi\pi^*$(keto)	m-m($\pi\pi^*$) 0−0($\pi\pi^*$)	3.53/3.51 3.39	3.09	3.48/3.38	3.22
nπ^*(enol)	m-m(nπ^*) 0−0(nπ^*)	3.72/3.70 3.58	3.24	3.74/3.60	
nπ^*(keto)	m-m(nπ^*) 0−0(nπ^*)	3.56/3.57 3.44	2.88	3.34/3.19	3.46
$\pi\pi^*$(keto)	fl($\pi\pi^*$)[g]	2.71/2.66 (52.3/54.3)	2.62 (112)	2.49/2.38	2.41 (2.4,[e] 2.5[d,f])
nπ^*(keto)	fl(nπ^*)[g]	2.63/2.64	2.03	1.92/1.76	2.35
nπ^*(enol)	fl(nπ^*)[g]	3.40/3.39	2.88	3.10/2.86	
$\pi\pi^*$(keto)	st($\pi\pi^*$)[h]	1.21/1.28	0.82	1.66/1.72	1.33 (1.5,[e] 1.4[d,f])
nπ^*(keto)	st(nπ^*)[h]	1.34/1.32	1.50	2.26/2.32	1.56
nπ^*(enol)	st(nπ^*)[h]	0.57/0.57	0.64	1.08/1.22	

[a] Oscillator strengths (absorption) and radiative lifetimes (ns) for fluorescence are given in parentheses for vertical $\pi\pi^*$ transitions. Oscillator strengths for nπ^* transitions are less than 10^{-3} and are not given in the table. [b] $\pi\pi^*$: $2^1A'$, nπ^*: $1^1A''$. [c] References 8 and 44. [d] Reference 37. [e] Reference 38. [f] Reference 39. [g] fl denotes vertical fluorescence transitions from the excited state to S_0. [h] st denotes the Stokes shift.

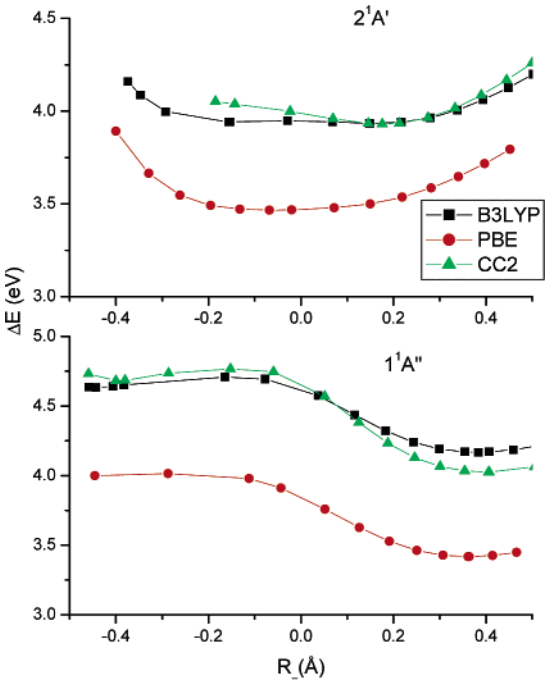

Figure 4. Proton-transfer curves for SA. Energies are given relative to the ground-state energy minimum.

nπ^* state the PBE excitation energy is also considerably lower than the B3LYP and RI-CC2 results. Unfortunately, in this case no CASPT2 results are available in the literature. All three methods give acceptable results for the fluorescence energy of the $\pi\pi^*$ state. In agreement with previous findings (see, e.g., ref 8), significant Stokes shifts are found due to the large geometry relaxation effects in the excited states.

C. Salicylic Acid. The proton-transfer curves for the $\pi\pi^*$ state (see Figure 4) are very flat, very similar to the situation found for OHBA. The assignment of an energy minimum

TABLE 3: TDDFT and RI-CC2 Vertical (vert) and Minimum-to-Minimum (m-m) and Zero-point Corrected (0−0) Absorption Energies (eV) for SA Relative to the Ground-State Energy Minimum, Oscillator Strengths, and Radiative Lifetimes[a]

geometry	transition[b]	B3LYP SVP/TZVP	PBE SVP	RI-CC2 SVP/TZVP	CASPT2[c] (exptl)
gr.st.	vert($\pi\pi^*$)	4.22/4.21 (0.08/0.08)	3.77 (0.06)	4.40/4.34	3.92 (3.9[d])
gr.st.	vert(nπ^*)	5.15/5.14	4.51	5.49/5.36	
$\pi\pi^*$(enol)	m-m($\pi\pi^*$) 0−0	3.94/3.93 3.76	3.47		
$\pi\pi^*$(keto)	m-m($\pi\pi^*$) 0−0	3.93/3.93 3.78	3.47	3.93/3.83	3.46 (3.69[e])
nπ^*(enol)	m-m(nπ^*) 0−0	4.63/4.61 4.45	4.00	4.68/4.50	
nπ^*(keto)	m-m(nπ^*) 0−0	4.17/4.18 4.02	3.42	4.03/3.88	
$\pi\pi^*$(enol)	fl($\pi\pi^*$)[g]	3.56/3.58 (22.7/22.5)	3.02 (50.5)		
$\pi\pi^*$(keto)	fl($\pi\pi^*$)[g]	3.03/2.95 (31.4/33.1)	3.01	2.82/2.72	2.83 (2.9,[f] 2.8[d])
nπ^*(enol)	fl(nπ^*)[g]	3.97/3.93	3.29	3.58/3.34	
nπ^*(keto)	fl(nπ^*)[g]	2.85/2.84	2.19	2.19/2.02	
$\pi\pi^*$(enol)	st($\pi\pi^*$)[h]	0.69/0.63	0.75		
$\pi\pi^*$(keto)	st($\pi\pi^*$)[h]	1.18/1.26	0.76	1.58/1.62	1.09 (1.0,[d] 1.1[f])
nπ^*(enol)	st(nπ^*)[h]	1.16/1.21	1.22	1.96/2.02	
nπ^*(keto)	st(nπ^*)[h]	2.20/2.30	2.32	3.30/2.34	

[a] Oscillator strengths (absorption) and radiative lifetimes (ns) for fluorescence are given in parentheses for vertical $\pi\pi^*$ transitions. Oscillator strengths for nπ^* transitions are less than 10^{-3} and are not given in the table. [b] gr.st.: $1^1A'$, $\pi\pi^*$: $2^1A'$, nπ^*: $1^1A''$. [c] Reference 8. [d] Reference 41. [e] Reference 40 [f] Reference 42. [g] fl denotes vertical fluorescence transitions from the excited state to S_0. [h] st denotes the Stokes shift.

structure is quite arbitrary. Formally, two local mimimum have been found at the B3LYP and PBE levels. The PT curves for the $1^1A''$(nπ^*) state show a relatively pronounced minimum for the keto structure. B3LYP and RI-CC2 vertical excitation energies seem to be somewhat too large (see Table 3). Available fluorescence data are quite well reproduced. For the Stokes shift in the $\pi\pi^*$ state, B3LYP gives good agreement with experiment and CASPT2 results.[8] Computed radiative lifetimes vary significantly between the B3LYP and PBE functionals demonstrating the difficulty for the accurate calculation of transition moments. Similar variations are found for the other molecules also. For comparison, the experimentally observed lifetime is 9.6 ns.[30] Comparison with the 33 ns of the B3LYP method shows agreement within realistic expectations, but also the need for improvement in this field.

D. 7-Hydroxy-1-indanone. Inspection of Figure 5 shows that for the $\pi\pi^*$ state an energy minimum exists for the keto form. The $1^1A''$(nπ^*) state has two distinct minima, one for the enol and one for the keto structure. Vertical excitation energies are displayed in Table 4. The PBE result is too low and the B3LYP/RI-CC2 values are too high. The PBE m-m excitation energy for the $\pi\pi^*$ state is too low as compared to the CASPT2 result. The fluorescence data for the $\pi\pi^*$ state are quite well reproduced. The Stokes shift is significantly overemphasized by the RI-CC2 method.

E. 2-(2′-Hydroxyphenyl)benzothiazole. HBT is the largest compound studied in this work. In this case CASPT2 benchmark calculations are not available anymore. PT curves are presented in Figure 6. As in the previous cases, the curve for the $\pi\pi^*$ state is very flat as compared to that for the nπ^* state. For the $\pi\pi^*$ state, only for the keto form was an energy minimum found, in contrast to the CIS optimization performed by Vivie-Riedle

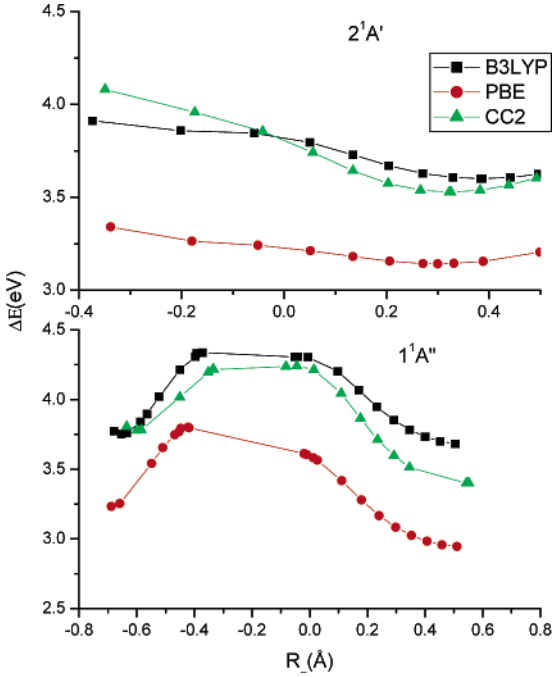

Figure 5. Proton-transfer curves for 7HIN. Energies are given relative to the ground-state energy minimum.

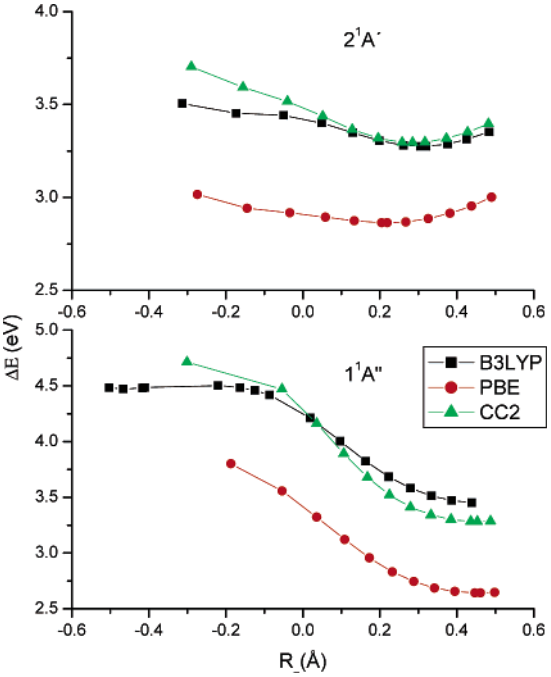

Figure 6. Proton-transfer curves for HBT. Energies are given relative to the ground-state energy minimum.

TABLE 4: TDDFT and RI-CC2 Vertical (vert) and Minimum-to-Minimum (m-m) and Zero-Point Corrected (0−0) Absorption Energies (eV) for 7HIN Relative to the Ground-State Energy Minimum, Oscillator Strengths, and Radiative Lifetimes[a]

geometry	transition[b]	B3LYP SVP/TZVP	PBE SVP	RI-CC2 SVP/TZVP	CASPT2[c] (exptl)
gr.st.	vert(nπ*)	4.03/4.02	3.59	4.20/4.11	
gr.st.	vert(ππ*)	4.13/4.13 (0.07/0.07)	3.61 (0.05)	4.33/4.29	3.89 (3.8[d], 3.9[e])
nπ*(enol)	m-m	3.75/3.75	3.23	3.78/3.64	
	0−0	3.64			
nπ*(keto)	m-m	3.68/3.69	2.94	3.40/3.25	
	0−0	3.58			
ππ*(keto)	m-m	3.60/3.58	3.18	3.53/3.42	3.37
	0−0	3.48			
nπ*(enol)	fl(nπ*)[f]	3.38/3.37	2.73	3.14/2.89	
nπ*(keto)	fl(nπ*)[f]	2.59/2.61	1.93	1.76/1.61	
ππ*(keto)	fl(ππ*)[f]	2.59/2.54 (49.1/51.0	2.33 (84.9)	2.33/2.21	2.36(2.4[d])
nπ*(enol)	st(nπ*)[g]	0.65/0.76	0.86	1.06/1.22	
nπ*(keto)	st(nπ*)[g]	1.44/1.41	1.66	2.44/2.50	
ππ*(keto)	st(ππ*)[g]	1.54/1.48	1.28	2.00/2.08	1.53 (1.4,[d] 1.5[e])

[a] Oscillator strengths (absorption) and radiative lifetimes (ns) for fluorescence are given in parentheses for vertical ππ* transitions. Oscillator strengths for nπ* transitions are less than 10^{-3} and are not given in the table. [b] gr.st.: $1^1A'$, ππ*: $2^1A'$, nπ*: $1^1A''$. [c] Reference 8. [d] Reference 37. [e] Reference 40. [f] fl denotes vertical fluorescence transitions from the excited state to S_0. [g] st denotes the Stokes shift.

et al.[11] The CIS method shows a pronounced minimum for the enol structure separated by a barrier of about 2 eV from the keto form. However, this barrier is reduced drastically when TDDFT energies are computed with use of CIS geometries. The enol minimum still remains, but the barrier is reduced to about 0.1−0.2 eV. Evidently, full TDDFT optimizations performed here let this minimum vanish completely. The B3LYP/RI-CC2 vertical ππ* excitation energies (see Table 5) agree well with the experimental value. All methods give good results for the ππ* fluorescence. The Stokes shift is significantly overestimated by the RI-CC2 method.

TABLE 5: TDDFT and RI-CC2 Vertical (vert) and Minimum-to-Minimum (m-m) and Zero-Point Corrected (0−0) Absorption Energies (eV) for HBT Relative to the Ground-State Energy Minimum Oscillator Strengths and Radiative Lifetimes[a]

geometry	transition[b]	B3LYP SVP/TZVP	PBE SVP	RI-CC2 SVP/TZVP	exptl[c]
gr.st.	vert(ππ*)	3.67/3.72 (0.34/0.36)	3.19 (0.20)	3.94/3.94	3.68[c]
gr.st.	vert(nπ*)	4.95/4.99	4.31	5.30/5.30	
ππ*(keto)	m-m(ππ*)	3.27/3.27	2.86	3.29/3.26	
	0−0	3.15			
nπ*(enol)	m-m(nπ*)	4.47/4.48			
	0−0				
nπ*(keto)	m-m(nπ*)	3.45/3.48	2.69	3.28/3.20	
	0−0	3.34			
ππ*(keto)	fl(ππ*)[e]	2.54/2.53 (17.9/18.0)	2.25 (37.9)	2.38/2.31	2.29[c]
nπ*(enol)	fl(nπ*)[e]	3.85/3.83			
nπ*(keto)	fl(nπ*)[e]	2.50/2.56	1.79	1.79/1.72	
ππ*(keto)	st(ππ*)[f]	1.13/1.19	0.94	1.56/1.63	0.93[d]
nπ*(enol)	st(nπ*)[f]	1.10/1.16			
nπ*(keto)	st(nπ*)[f]	2.45/2.43	2.52	2.51/3.58	

[a] Oscillator strengths (absorption) and radiative lifetimes (ns) for fluorescence are given in parentheses for vertical ππ* transitions. Oscillator strengths for nπ* transitions are less than 10^{-3} and are not given in the table. [b] gr.st.: $1^1A'$, ππ*: $2^1A'$, nπ*: $1^1A''$. [c] Reference 43. [d] Reference 32. [e] fl denotes vertical fluorescence transitions from the excited state to S_0. [f] st denotes the Stokes shift.

IV. Structural Effects

Our discussion of structural changes due to electron excitation and proton-transfer concentrates on the chelate ring. Respective bond distances are given in the tables to be discussed below. Full Cartesian geometries can be found in the Supporting Information (see the end of the text for more information).

For malonaldehyde basis set effects on computed geometries have been investigated more extensively. Results are given in Table 6. Geometries have been optimized with use of C_s symmetry. The symmetrical C_{2v} structure of the ππ* state is well reproduced in the RI-CC2 calculations. The CO and CC double bonds are stretched due to the ππ* excitation in

TABLE 6: Selected Bond Distances (Å) Computed for Optimized Structures of MA[a]

	O_1H_1	O_2H_1	O_1C_1	C_1C_2	C_2C_3	C_3O_2
B3LYP(SVP/TZVPP)						
gr.st.[0][b]	1.011/0.998	1.628/1.686	1.312/1.318	1.373/1.361	1.440/1.436	1.239/1.236
Rgs(nπ*)[c]	1.011/0.998	1.915/2.000	1.347/1.352	1.398/1.388	1.387/1.378	1.310/1.308
nπ*[0][b]	0.972/0.966	2.001/2.056	1.348/1.352	1.398/1.388	1.386/1.378	1.308/1.307
Rgs($\pi\pi$*)[c]	1.011/0.998	1.577/1.620	1.317/1.320	1.433/1.424	1.475/1.466	1.274/1.273
$\pi\pi$*[1][b]	1.104/0.998	1.421/1.692	1.309/1.317	1.438/1.361	1.468/1.436	1.281/1.236
PBE(SVP/TZVPP)						
gr.st.	1.058/1.040	1.487/1.543	1.309/1.316	1.388/1.376	1.433/1.429	1.259/1.256
nπ*	0.977/0.972	2.117/2.142	1.355/1.359	1.433/1.422	1.374/1.367	1.305/1.308
$\pi\pi$*	1.137/1.114	1.387/1.424	1.319/1.325	1.430/1.420	1.494/1.486	1.288/1.288
RI-CC2(SVP/TZVPP)						
gr.st.	1.017/1.018	1.590/1.569	1.318/1.321	1.379/1.371	1.437/1.428	1.254/1.259
nπ*[d]	0.987/0.983	1.726/1.741	1.352/1.358	1.403/1.397	1.376/1.362	1.410/1.429
	(0.964)	(2.064)	(1.369)	(1.393)	(1.398)	(1.355)
$\pi\pi$*[d]	1.236/1.233	1.235/1.236	1.320/1.326	1.456/1.446	1.457/1.446	1.320/1.326
	(1.221)	(1.221)	(1.312)	(1.458)	(1.458)	(1.312)

[a] For the numbering scheme see Figure 1. [b] Number of imaginary frequencies given in brackets. [c] O_1H_1 bond distance fixed to the ground-state value. [d] MR-AQCC values[9] in parentheses.

comparison to the ground-state values. Basis set effects are rather small. Larger ones are observed for some of the B3LYP and PBE bond distances of the $\pi\pi$* state. The $\pi\pi$* state is the most critical case for the DFT methods since the correct C_{2v} symmetry is not reproduced by B3LYP and PBE. The most remarkable geometry change due to the nπ* excitation is the strong stretching of the C_3O_2 bond to 1.429 Å by the RI-CC2 method. The adjacent C_2C_3 bond is shortened and the C_1C_2 bond is stretched as compared to the ground-state geometry. Similar effects are observed for the B3LYP and PBE methods also. Only the stretching of the CO bond is not so pronounced. The MR-AQCC C_3O_2 bond distance (1.355 Å) is given in Table 6 for comparison. This value is about midway between the B3LYP and RI-CC2 results. Thus, RI-CC2 overestimates the length of this bond distance. The CASSCF geometry parameters[27] (in particular the C_3O_2 bond distance of 1.361 Å) are in very good agreement with the MR-AQCC results. This fact is encouraging in view of the larger ESIPT systems, where MR-AQCC calculations could not be carried out so far. The PBE results agree quite well with the B3LYP data. Generally, the performance of the DFT and RI-CC2 methods is quite acceptable. This is not the case for the CIS results reported by Cuma et al.,[31] e.g., the C_3O_2 bond length in the nπ* state is computed as 1.257 Å, a value that is much too short. The remaining CIS geometry data are also not encouraging.

After this methodological discussion for malonaldehyde, a systematic comparison of structural changes will be carried out for all systems considered in this work. This discussion will be restricted to the results obtained with the B3LYP and RI-CC2 methods. The geometry changes along the PT path are split up into two steps. In the first step we investigate the changes in the enol form due to the electronic excitation. Since in most cases the enol structure is not well defined as the minimum-energy structure, we decided to choose as reference an enol structure where the OH bond distance was fixed to the ground-state value and the remaining geometry parameters were optimized for the respective state. This structure will be denominated as Rgs in the following discussion. Comparison of ground-state and Rgs structures shows (see Tables 6−10) that significant geometric relaxation effects occur already at this level for all systems investigated. The major effect is the increase of the C_3O_2 bond. The C_1O_1 counterpart is not affected so much. It is increased slightly in the nπ* state and is somewhat decreased in the $\pi\pi$* state. The hydrogen bond O_2H_1 decreases significantly in the $\pi\pi$* state, thus strengthening the hydrogen bond as compared to the ground state. On the other side, the O_2H_1 bond increases in the nπ* state.

In the second step, relaxation to the keto form is considered. In the course of the PT further geometrical adjustments occur. In the $\pi\pi$* state the C_3O_2 distance is further increased and the O_1C_1 distance is decreased in comparison to the Rgs structure (B3LYP results). Finally, at the B3LYP level, the O_1C_1 distance is smaller by about 0.05 Å than in the ground state. The RI-CC2 values are slightly different showing almost no change in the O_1C_1 distance between $\pi\pi$* and the ground state. For the

TABLE 7: Selected Bond Distances (Å) Computed for Optimized Structures of OHBA, Using the TZVP Basis Set[a]

	O_1H_1	O_2H_1	O_1C_1	C_1C_2	C_2C_3	C_3O_2
B3LYP						
gr.st.[0][b]	0.986	1.759	1.340	1.417	1.452	1.228
Rgs(nπ*)[c]	0.986	1.843	1.360	1.439	1.392	1.306
nπ*(enol)[0][b]	0.970	1.875	1.361	1.439	1.392	1.306
nπ*(keto)[0][b]	1.792	0.976	1.319	1.450	1.400	1.340
Rgs($\pi\pi$*)[c]	0.986	1.592	1.323	1.435	1.471	1.275
$\pi\pi$*(keto)[1][b]	1.548	1.038	1.281	1.443	1.443	1.314
RI-CC2						
gr.st.	0.992	1.715	1.348	1.416	1.452	1.246
nπ*(enol)	0.986	1.683	1.367	1.437	1.383	1.426
nπ*(keto)	1.782	0.981	1.434	1.426	1.413	1.358
$\pi\pi$*(keto)	1.457	1.078	1.349	1.444	1.463	1.319

[a] For the numbering scheme see Figure 1. [b] Number of imaginary frequencies given in brackets. [c] O_1H_1 bond distance fixed to the ground-state value.

TABLE 8: Selected Bond Distances (Å) Computed for Optimized Structures of SA, Using the TZVP Basis Set[a]

	O_1H_1	O_2H_1	O_1C_1	C_1C_2	C_2C_3	C_3O_2
B3LYP						
gr.st.[0][b]	0.983	1.754	1.343	1.416	1.463	1.226
Rgs(nπ*)[c]	0.983	1.883	1.369	1.441	1.375	1.331
nπ*(enol)[1][b]	0.966	1.916	1.369	1.442	1.375	1.330
nπ*(keto)[1][b]	1.795	0.973	1.331	1.444	1.404	1.345
Rgs($\pi\pi$*)[c]	0.983	1.618	1.325	1.497	1.444	1.264
$\pi\pi$*(enol)[0]	1.058	1.472	1.319	1.447	1.444	1.273
$\pi\pi$*(keto)[0][b]	1.451	1.070	1.291	1.451	1.441	1.311
RI-CC2						
gr.st.	0.987	1.728	1.351	1.415	1.463	1.239
nπ*(enol)	0.974	1.812	1.379	1.436	1.374	1.448
nπ*(keto)	1.813	0.976	1.431	1.430	1.403	1.362
$\pi\pi$*(keto)	1.431	1.080	1.344	1.460	1.438	1.320

[a] For the numbering scheme see Figure 1. [b] Number of imaginary frequencies given in brackets. [c] O_1H_1 bond distance fixed to the ground-state value.

TABLE 9: Selected Bond Distances (Å) Computed for Optimized Structures of 7HIN, Using the TZVP Basis Set[a]

	O_1H_1	O_2H_1	O_1C_1	C_1C_2	C_2C_3	C_3O_2
B3LYP						
gr.st.[0][b]	0.979	1.980	1.347	1.402	1.453	1.225
Rgs($n\pi^*$)[c]	0.979	2.289	1.367	1.427	1.390	1.290
$n\pi^*$(enol)[0][b]	0.964	2.304	1.367	1.427	1.390	1.290
$n\pi^*$(keto)[0][b]	2.137	0.969	1.322	1.433	1.399	1.343
Rgs($\pi\pi^*$)[c]	0.979	1.798	1.327	1.411	1.442	1.271
$\pi\pi^*$(keto)[0][b]	1.872	1.001	1.272	1.426	1.430	1.327
RI-CC2						
gr.st.	0.983	1.957	1.354	1.401	1.453	1.242
$n\pi^*$(enol)	0.971	2.210	1.372	1.424	1.380	1.404
$n\pi^*$(keto)	2.141	0.975	1.439	1.412	1.410	1.359
$\pi\pi^*$	1.724	1.028	1.339	1.422	1.444	1.331

[a] For the numbering scheme see Figure 1. [b] Number of imaginary frequencies given in brackets. [c] O_1H_1 bond distance fixed to the ground-state value.

TABLE 10: Selected Bond Distances (Å) Computed for Optimized Structures of HBT, Using the TZVP Basis Set[a]

	O_1H_1	NH_1	O_1C_1	C_1C_2	C_2C_3	C_3N
B3LYP						
gr.st.[0][b]	0.990	1.753	1.343	1.420	1.453	1.304
Rgs($n\pi^*$)[c]	0.990	1.907	1.366	1.434	1.399	1.336
$n\pi^*$(enol)[−][b]	0.969	1.959	1.367	1.434	1.400	1.335
$n\pi^*$(keto)[1][b]	1.958	1.012	1.330	1.437	1.426	1.374
Rgs($\pi\pi^*$)[c]	0.990	1.657	1.321	1.459	1.432	1.348
$\pi\pi^*$(keto)[0]	1.733	1.044	1.276	1.461	1.457	1.351
RI-CC2						
gr.st.	0.995	1.716	1.350	1.420	1.450	1.322
$n\pi^*$(keto)	1.966	1.016	1.432	1.423	1.423	1.392
$\pi\pi^*$(keto)	1.682	1.058	1.331	1.462	1.460	1.369

[a] For the numbering scheme see Figure 1. [b] Number of imaginary frequencies given in brackets. [c] O_1H_1 bond distance fixed to the ground-state value.

$n\pi^*$ state, the RI-CC2 method predicts a stretching of the O_1C_1 bond by almost 0.1 Å for all cases except MA and HBT. Thus, the PT weakens this CO bond considerably. On the other hand, the B3LYP method shows a slight strengthening of this bond distance.

It is interesting to follow the changes in the framework of the aromatic ring system, as has been done before by Cuma et al.[31] A systematic pattern of strengthening of the C_2C_7 and C_5C_6 bonds and weakening of the C_6C_7 and C_4C_5 bonds is observed for the $\pi\pi^*$ state as compared to the ground-state structure. In the case of the $n\pi^*$ state the pattern of bond stretches and shortenings in the aromatic ring system is less systematic.

The number of imaginary frequencies is given in Tables 6−10 also. Most of the $\pi\pi^*$ keto structures (except OHBA) are minima. The $n\pi^*$ structures of SA and HBT are saddle points. The out-of-plane modes corresponding to the imaginary frequency are motions within the chelate ring.

The structural changes during the ESIPT refer primarily to the motion of the proton from the donor to the acceptor atom. This motion is described directly by the coordinates R_{OH} and R_-, respectively. However, the PT is strongly coupled to other internal coordinates. This multidimensionality of the PT process has already been stressed in the review presented by Douhal et al.[7] The importance of the coupling of the OH stretching with the ON distance has been clearly demonstrated for HBT by Lochbrunner et al.[32] and Vivie-Riedle et al.[11] and for the OO distance in OHBA by Stock et al.[33] The dependence of the O_1O_2 distance on R_- is shown in Figure 7 for both the $\pi\pi^*$ and $n\pi^*$ states. A reduction of the O_1O_2 distance is found during the early stages of the PT followed by a subsequent elongation. A more detailed analysis of the vibrational modes shows a more

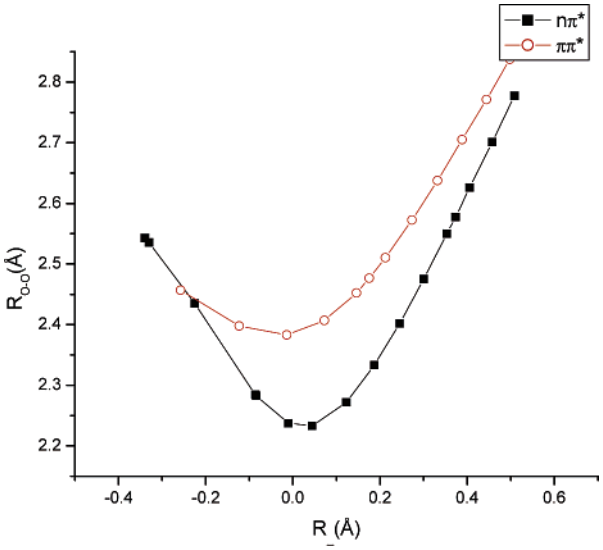

Figure 7. Dependence of O_1O_2 on R_- for OHBA.

or less rigid approach of the proton donor and proton acceptor moieties followed by the PT. This behavior is typical for all PT systems investigated here and agrees very nicely with the analysis of Vivie-Riedle et al.[11] for the $\pi\pi^*$ state of HBT. However, we want to stress that this PT mechanism is not only characteristic for the $\pi\pi^*$ state but is, as Figure 7 shows, also valid for the $n\pi^*$ state.

V. Conclusions

Systematic investigations on ESIPT processes have been performed on several molecular systems starting from the relatively small malonaldehyde up to (2′-hydroxyphenyl)-benzothiazole with the TDDFT and RI-CC2 methods. Complete geometry optimizations have been performed under planarity restriction in the excited states allowing internally consistent descriptions of stationary points and proton-transfer curves. Comparison with existing experimental and CASPT2/MR-AQCC data has to be made with care since (a) computed vertical excitation energies cannot be related directly to band maxima and (b) the higher level benchmark methods are also submitted to nonnegligible errors due to the large size of the molecular systems. In critical cases, such as the symmetry of the $\pi\pi^*$ state of malonaldehyde, RI-CC2 is more reliable than TDDFT. However, we note by comparison with MR-AQCC results that RI-CC2 has a tendency to overshoot bond changes due to electron excitation in certain situations. In summary, we have shown that both RI-CC2 and TDDFT are viable candidates for the description of energy surfaces for ESIPT processes. Naturally, the TDDFT approach is the much faster method. However, it is advantageous to have alternative methods of competitive efficiency available to check the TDDFT results. As concerns the choice of the DFT functional, we favor B3LYP because of its proximity to RI-CC2 energies. Additionally, in view of the huge popularity of B3LYP we do not see any reason to discourage its use because of shortcomings in selected points. If computational efficiency is really an issue, the RI-PBE combination is an interesting alternative. In most cases, PT curves computed with PBE are shifted by about 0.5 eV to lower values, but always are closely parallel to the B3LYP/RI-CC2 curves.

On the ground-state energy surface only an enol minimum structure has been observed. Attempts to locate a keto minimum always led back to the enol form. Both the $n\pi^*$ and $\pi\pi^*$ states

have been studied at equal footing. Energetically, both states are very close to each other at both the enol and the keto side of the PT process. Excitation to the $\pi\pi^*$ state is, of course, preferred due to dominating oscillator strengths. In the case of the $\pi\pi^*$ state the PT curves are very shallow with minima mostly located on the keto side. For salicylic acid two minima have been located, separated only by an extremely small barrier. Thus, the picture of an intramolecular vibrational relaxation process without barrier given by Sobolewski and Domcke[8] is confirmed. The PT process is strongly coupled to rigid motions bringing the migrating hydrogen atom close to the acceptor atom as has been shown by Vivie-Riedle et al.[11] for the $\pi\pi^*$ state of HBT. The role of the nπ^* state in the PT process is not so clear yet. Two minima (under planarity restriction) for the enol and keto form are found. Depending on the case, energy barriers ranging from values <0.1 eV up to 0.5 eV were observed. In contrast to the $\pi\pi^*$ state, a definite preference for the keto form is observed. From our PT curves one can see that crossings between the two states will occur at various stages of the PT process. Out-of-plane motions will couple the two states. Crossings and recrossings are conceivable. Hydrogen detachment processes[34] leading to conical intersections are certainly also possible for the nπ^* state. Dynamics calculations are required for a detailed evaluation of these questions and of the ESIPT process as a whole. This work should have provided one step further toward this ultimate goal.

Acknowledgment. The authors acknowledge support by the Austrian Science Fund within the framework of the Special Research Program F16 and Project P14817-N03. The calculations were performed in part on the Schrödinger II cluster of the University of Vienna.

Supporting Information Available: Total energies and Cartesian coordinates for the stationary points investigated. This material is available free of charge via the Internet at http://pubs.acs.org.

References and Notes

(1) Acuña, A. U.; Costela A.; Muñoz, J. M. *J. Phys. Chem*. **1986**, *90*, 2807.
(2) Chou, P. T.; McMorrow, D.; Kasha, M. *J. Phys. Chem*. **1984**, *88*, 4596.
(3) Parthenopoulos, D. A.; McMorrow, D.; Kasha, M. *J. Phys. Chem*. **1991**, *95*, 2668.
(4) Catalan, J.; Delvalle, J. C.; Fabero, F.; Garcia, N. A. *Photochem. Photobiol.* **1995**, *61*, 118.
(5) Keck, J.; Kramer, H. E. A.; Port H.; Hirsch, T.; Fischer, P.; Rytz, G. *J. Phys. Chem.* **1996**, *100*, 14468.
(6) Catalán, J.; Fabero, F.; Guijarro, M. S.; Claramunt, R. M.; Santa-María, M. D.; Foces-Focess, M. C.; Hernández-Cano, F.; Elguero J.; Sastre, R. *J. Am. Chem. Soc*. **1990**, *112*, 747.
(7) Douhal, A.; Lahmani, F.; Zewail, A. H. *Chem. Phys*. **1996**, *207*, 477.
(8) Sobolewski, A. L.; Domcke, W. *Phys. Chem. Chem. Phys.* **1999**, *1*, 3065.
(9) Monte, S. A. do; Dallos, M.; Müller, Th.; Lischka, H. *Collect. Czech. Chem. Commun*. **2003**, *68*, 447.
(10) Sobolewski, A. L.; Domcke, W. *Ultrafast Hydrogen Bonding Dynamics and Proton-Transfer Processes in the Condensed Phase*; Understanding Chemical Reactivity Series; Elsaesser, T. H., Bakker, H. J., Eds.; Kluwer Academic Publishers: Boston, MA, 2003; Vol. 23, p 93.
(11) Vivie-Riedle, R. de; De Waele, V.; Kurtz, L.; Riedle, E. *J. Phys. Chem. A* **2003**, *107*, 10591.
(12) Furche, F.; Ahlrichs R. *J. Chem. Phys*. **2002**, *117*, 7433.
(13) Dreuw, A.; Head-Gordon, M. *J. Am. Chem. Soc*. **2004**, *126*, 4007.
(14) Christiansen, O.; Koch, H.; Jørgensen, P. *Chem. Phys. Lett*. **1995**, *243*, 409.
(15) Köhn, A.; Hättig, C. *J. Chem. Phys*. **2003**, *119*, 5021.
(16) Hättig, C. *J. Chem. Phys*. **2003,** *118*, 7751.
(17) Granucci, G.; Persico, M.; Toniolo, A. *J. Chem. Phys*. **2001**, *114*, 10608.
(18) Barbatti, M.; Granucci, G.; Persico, M.; Lischka, H. *Chem. Phys. Lett*., **2005**, *401*, 276.
(19) Ahlrichs, R.; Bär, M.; Häser, M.; Horn, H.; Kölmel, C. *Chem. Phys. Lett.* **1989**, *162*, 165.
(20) Bauernschmitt, R.; Ahlrichs R. *Chem. Phys. Lett.* **1996**, *256*, 454.
(21) Bauernschmitt, R.; Häser, M.; Treutler, O.; Ahlrichs, R. *Chem. Phys. Lett.* **1997**, *264*, 573.
(22) Becke, A. D. *J. Chem. Phys*. **1993**, *98*, 5648.
(23) Perdew, J. P.; Burke, K.; Ernzerhof, M. *Phys. Rev. Lett* **1997**, *78*, 1386.
(24) Schäfer, A.; Horn, H.; Ahlrichs, R. *J. Chem. Phys.* **1992**, *97*, 2571.
(25) Schäfer, A.; Huber, C.; Ahlrichs, R. *J. Chem. Phys.* **1994**, *100*, 5829.
(26) Weigend, F.; Häser, M.; Patzelt, H.; Ahlrichs, R. *Chem. Phys. Lett*. **1998**, *294*, 143.
(27) Sobolewski, A. L.; Domcke, W. *J. Phys. Chem. A* **1999**, *103*, 4494.
(28) Brandsen, B. H.; Joachain, C. J. *Physics of Atoms and Molecules*; Longman Group Limited, 1983.
(29) Rowe, W. F.; Duerst, R. W.; Wilson, E. B. *J. Am. Chem Soc*. **1978**, *98*, 4021.
(30) Bisht, P. B.; Petek, H.; Yoshihara, K.; Nagashima, U. *J. Chem. Phys*. **1995**, *103*, 5290.
(31) Cuma, M.; Scheiner, S.; Kar, T. *J. Mol. Struct.* (*THEOCHEM*) **1999**, *467*, 37.
(32) Lochbrunner, S.; Wurzer, A. J.; Riedle, E. *J. Phys. Chem. A* **2003**, *107*, 10580.
(33) Stock, K.; Bizjak, T.; Lochbrunner, S. *Chem. Phys. Lett*. **2002**, *354*, 409.
(34) Sobolewski, A. L.; Domcke, W. *Chem. Phys*. **2000**, *259*, 181.
(35) Seliskar, C. J.; Hoffmann, R. E. *J. Mol. Spectrosc*. **1981**, *88*, 30.
(36) Firth, D. W.; Barbara, P. F.; Trommsdorf, H. P. *Chem. Phys*. **1989**, *136*, 349.
(37) Nagaoka, S.; Hirota, N.; Sumitani, M.; Yoshihara, K.; Lipczynska-Kochany, E.; Iwamura, H. *J. Am. Chem. Soc*. **1984**, *106*, 6913.
(38) Nagaoka, S.; Nahashima, U. *Chem. Phys*. **1989**, *136*, 153.
(39) Morgan, M. A.; Orton, E.; Pimentel, G. C. *J. Phys. Chem*. **1990**, *94*, 7927.
(40) Nishiya, T.; Yamauchi, S.; Hirota, M.; Baba, M.; Hanazaki, I. *J. Phys. Chem.* **1986**, *90*, 5730.
(41) Pant, D. D.;, Joshi, H. C.; Bisht, P. B.; Tripathi, H. B. *Chem. Phys*. **1994**, *185*, 137.
(42) Lahmani, F.; Zehnacker-Rentien, A. *Chem. Phys. Lett*. **1997**, *271*, 6.
(43) Lochbrunner, S.; Wurzer, A. J.; Riedle, E. *J. Chem. Phys.* **2000**, *112*, 10699.
(44) Sobolewski, A. L.; Domcke, W. *Chem. Phys*. **1994**, *184*, 115.